Journal of Photochemistry & Photobiology, B: Biology 180 (2018) 218–224

Contents lists available at ScienceDirect

Journal of Photochemistry & Photobiology, B: Biology

journal homepage: www.elsevier.com/locate/jphotobiol

Laser assisted anticancer activity of benzimidazole based metal organic nanoparticles

P.A. Praveen[a], R. Ramesh Babu[a,*], P. Balaji[b], A. Murugadas[b], M.A. Akbarsha[b]

[a] Crystal Growth and Thin Film Laboratory, Department of Physics, Bharathidasan University, Tiruchirappalli 620 024, Tamilnadu, India
[b] National Centre for Alternatives to Animal Experiments, Bharathidasan University, Tiruchirappalli 620 024, Tamilnadu, India

ARTICLE INFO

Keywords:
Photothermal therapy
Nonlinear absorption
Laser
Cancer

ABSTRACT

Recent studies showed that the photothermal therapy can be effectively used for the targeted cancerous cells destruction. Hence, in the present study, benzimidazole based metal organic complex nanoparticles, dichloro cobalt(II) bis-benzimidazole (Co-BMZ) and dichloro copper(II) bis-benzimidazole (Cu-BMZ), were synthesized by reprecipitation method and their anti-cancer activity by means of photothermal effect has been studied. Transmission electron microscopy analysis shows that the particle size of Cu-BMZ is ~100 nm and Co-BMZ is in the range between 100 and 400 nm. Zeta potential analysis ensures the stability of the synthesized nanoparticles. It is found that the nonlinear absorption of the nanoparticles increases with increase in laser power intensity. Phototoxicity of human lung cancer (A549) and the normal mouse embryonic fibroblast (NIH-3T3) cells was studied using a 650 nm laser. Even though both the cell lines were affected by laser irradiation, A549 cells show higher cell destruction and lower IC_{50} values than the normal cells. Docking studies were used to analyse the interaction site and the results showed that the Cu-BMZ molecules have higher dock score than the Co-BMZ molecules. The obtained results indicate that Cu-BMZ samples have lesser particle size, higher nonlinear absorption and higher interaction energy than the Co-BMZ samples.

1. Introduction

Cancer is one of the deadlier diseases that accounts for millions of death every year. In 2016, it is estimated that 1,685,210 new cases are diagnosed with cancer and it caused death of 595,690 people in US alone [1]. There are different types of cancer such as, leukemia, melanoma, non-Hodgkin lymphoma, breast cancer, thyroid cancer, lung and bronchus cancer, kidney and renal pelvis cancer, etc., which may all ultimately lead to death. The widely used chemical and radiation therapies are not only ineffective in advanced stages, but also creates additional side effects to the patients [2–4]. Hence, much efforts are required to develop alternate therapeutic strategies which could effectively treat the disease with no or minimum side effects. Photothermal therapy (PTT) is one such therapeutic strategy with high efficacy and low complications [5]. The advantage of this method includes the minimal invasion, low systemic toxicity, spatio-temporal controllability and limited side effects [6,7]. In PTT, the malignant cells were destroyed by the locally induced heating effect by light energy sources, most often a laser. The major issue in PTT is that the treatment is non-local or non-target specific and can destroy both the benign and malignant cells [5]. For target specific treatment in PTT often a photoabsorber or a transducer is considered. These bridging molecules should have strong absorption in the wavelength of light source, often a NIR (600–900 nm) source due to their high penetration depths [8] and capable of binding with the malignant cells alone. Thus they offer selective destruction of abnormal cells over a region, leads to precise and minimally invasive alternative treatment. The design strategy for an effective therapy is to synthesize a photothermal transducer that should have high absorption in the operating wavelength of the light source and could effectively convert the absorbed light into heat without any local radiative process [9].

In the recent past many materials including organic dyes, inorganic nanomaterials, metal chalcogenides and carbon based materials with the aforementioned properties are investigated in this regard [10–14]. In which, organic materials possess certain advantages, such as biocompatibility and biodegradability, to treat humans. Further they offer wide variety of tailoring possibilities so that a drug can be integrated towards different treating points [15]. On the other hand organic materials possess certain disadvantages such as low photo to thermal conversion efficiency, poor thermal stability and complicated synthesis process, which limits their possibilities for PTT [16]. One strategy to improve the physical stability and conversion efficiency of organic

* Corresponding author.
E-mail addresses: rampap2k@yahoo.co.in, rameshbabu.r@bdu.ac.in (R. Ramesh Babu).

https://doi.org/10.1016/j.jphotobiol.2018.02.008
Received 12 December 2017; Received in revised form 17 January 2018; Accepted 7 February 2018
Available online 09 February 2018
1011-1344/

materials is, incorporation of metal ions in the organic medium and fabricate them as metal-organic complexes. The metal ions with organic ligands possess improved physical properties and often give rise to additional energy levels, which in turn increases the photothermal conversion efficiency of the material [17–20].

Benzimidazole (BMZ) is a well known antibacterial agent and its derivatives have been widely investigated for the development of cancer drugs [21,22]. Further, the BMZ complexes gain much attention in the materials science regime for photonics related applications. Especially, the transition metal complexes of BMZ show good thermo-optical properties in the 650 nm region [17]. In the consideration of PTT, the first step to develop a potential PTT transducer, that has to have the capability to bind with the target, absorb enough energy and kill maximum malignant cells [23] and of course, it should not (or very lesser) interact with the normal cells. Hence, in the present work, BMZ metal complexes, based on cobalt and copper, have been investigated for PTT. The metal complexes, dichloro cobalt(II) bis-benzimidazole (Co-BMZ) and dichloro copper(II) bis-benzimidazole (Cu-BMZ) complexes were synthesized as nanoparticles by reprecipitation method. They were subjected to morphological, linear and nonlinear optical studies and their PTT efficiency is studied by exposing them to NIH/3T3 and A549 cell lines. Further, their molecular binding site with A549 cells is analysed by means of docking studies.

2. Materials and Methods

2.1. Material Synthesis

All the raw materials used for the synthesis of Co-BMZ and Cu-BMZ complexes were reagent grade and purchased from Merck chemicals. For the synthesis, respective metal chlorides ($CoCl_2 \cdot 6H_2O$ and $CuCl_2 \cdot 2H_2O$) and ligand (BMZ) were taken in 1:2 ratio and dissolved in ethanol separately. The BMZ solution was transferred to a glass container and heated at 70 °C for an hour. Then the metal solution (either cobalt or copper chloride solution) was added dropwise into the BMZ solution. This solution was refluxed for 24 h and transferred to another beaker kept at room temperature. After cooling, the beaker was covered with aluminum foil and kept undisturbed for a week. Thereupon, either blue or green precipitate was obtained depending upon the metal solution utilized. The purity of the final product was ensured by means of column chromatography and the molecular structure of the complexes were confirmed by FTIR analysis (not given here). Further, these powdered samples were used for the preparation of nanoparticles.

2.2. Nanoparticle Synthesis

For the preparation of nanoparticles, a reprecipitation method was employed and the details can be found elsewhere [24]. The idea is by rapidly mixing the solution of the target material to a solvent, where the solubility of the material is very poor or non-soluble and at the same time the solvent should dissolve well with the poor solvent. This situation leads to rapid precipitation of the target material. In the present work, water was chosen as the poor solvent and was kept above 70 °C for better results. The product (either Co-BMZ or Cu-BMZ) was dissolved in methanol and the solution was filtered many times to obtain a clear solution without any undissolved powder/particles. Then the solution was loaded in a syringe with needle of diameter less than 1 micron. This solution was rapidly sprayed on to the water. The obtained colloidal suspension is stable for several weeks and was used for the further characterization studies.

2.3. Characterization Studies

Dynamic light scattering (DLS) and zeta-potential of the samples were measured using Malvern Zetasizer Nano ZS ZEN 3600 instrument. All the measurements were carried out at 25 °C. About 1 ml of the colloidal solution was transferred to a clean, light-scattering cell. Transmission electron microscopy (TEM) analysis was performed using a Philips CM20 instrument with an accelerating voltage about 200 kV. GeneQuant 1300 UV-Vis. spectrophotometer was used to record the absorptive behavior of the samples in the range between 300 and 900 nm. The nonlinear thermo-optical behavior of the samples was studied by means of Z-scan technique. A diode laser of power 20 mW and the Gaussian profile at 650 nm was used as the source. There are two possible configurations in Z-scan, (i) open aperture (OA) and (ii) closed aperture (CA) scans corresponding to nonlinear absorptive and refractive coefficients of the samples. The OA and CA Z-scan curves of the nanoparticles were recorded at different power densities, between 1 and 5 mW, and from that data third order nonlinear susceptibility of the samples was calculated. The corresponding experimental details and fitting parameters are discussed elsewhere [17].

2.4. Anticancer Studies

2.4.1. Cell Culture

The human lung cancer cell line (A549) and mouse embryonic fibroblast cell lines (NIH-3T3) were obtained from the National Center for Cell Science (NCCS), Pune, India. The cells were cultured in DMEM high glucose medium (Sigma-Aldrich, USA) supplemented with 10% fetal bovine serum (Gibco), and 20 ml of penicillin/streptomycin as antibiotics (Gibco), in a culture flask at 37 °C in a humidified atmosphere of 5% CO_2 in a CO_2 incubator (Thermo scientific, USA). All the culture experiments were performed in cells from passage 15 or less.

2.4.2. Cell Viability Assay

To study the cytotoxic effect of Cu-BMZ and Co-BMZ complexes against both cell types, the nanoparticles were dissolved in 100% dimethyl sulfoxide (DMSO) and diluted to obtain a final concentration of 0.02%. This was added to the 96 well plate, containing 5×10^3 cells per well. In order to study the phototoxic effect of laser (against the cells), the cells were treated with different laser powers, between 1 and 5 mW, for 4 min and the corresponding cell death was analysed using MTT assay. DMSO was used as the solvent control. After the addition of nanoparticles to the plate, the cells were irradiated with laser light (Power = 5 mW) at 25 °C for 4 min and then the plates were incubated for 24 h at 37 °C. The same procedure was followed without light irradiation to determine the effect of laser induced cell death. After 24 h of incubation, 20 µl of MTT solution (5 mg/ml in PBS) was added and the plates were wrapped with aluminum foil and incubated for 4 h at 37 °C. The produced purple formazan product was dissolved by addition of 100 µl of DMSO and the absorbance was recorded at 570 nm (measurement) and 630 nm (reference) using a 96-well plate reader (Bio-Rad, iMark, USA). Data collected from the three replicates were used to calculate the respective mean, and the percentage of cell viability was calculated using the formula [25]:

$$\frac{\text{Mean of absorbance of untreated cells (Control) - Mean of absorbance of treated cells}}{\text{Mean of absorbance of untreated cells (Control)}} \times 100 \quad (1)$$

2.5. Morphological Observations

2.5.1. Light Microscopic Study and Acridine Orange (AO) and Ethidium Bromide (EB) Staining

Induction of apoptosis by metal organic nanoparticles was investigated by AO/EB double staining method as described by Spector et al. with some modifications [26]. Briefly, sub-confluent monolayer culture of A549 and NIH-3T3 cells was trypsinized and 5×10^5 cells/ml were seeded into 6 well plate containing cover slip. The cells were treated with IC_{50} concentration of nanoparticles irradiated for 4 min and incubated for 24 h. After the incubation period, 25 µl of AO/EB

solution (3.8 μM of AO and 2.5 μM of EB in PBS) was added on to the cover slip and examined immediately under fluorescent microscope (Carl Zeiss, Axioscope2plus) with UV filter (450–490 nm). The cells treated with nanoparticles were also subjected directly under the light microscopy (Carl Zeiss, Axioscope2plus) for cytological changes.

2.6. Docking Methods

Autodock version 4.2.5.1 and Auto Dock Tools (ADT) version 1.5.6 were used for the docking calculations. The ALK protein was obtained from RSC's protein data bank (ID: 2XP2) and the co-crystallized ligand (criztinib) was removed prior to the input file preparation. Polar hydrogens and Gasteiger charges were added and the incomplete side chains were removed using ADT. Then the structure was saved in PDBQT format in order to use it as autodock input. The ligands were drawn using MarvinSketch and saved in MOL format. The structure was further optimized using UFF algorithm in Avogadro package and saved as MOP format for geometry optimization using MOPAC2012 package. The optimized structure was evaluated by vibrational analysis and the obtained all-positive vibrational peaks ensure the stability of the structure. This was then converted into PDB file using Avogadro and then to PDBQT using ADT for autodock analysis. The grid box for calculations was constructed using the grid size about $40 \times 40 \times 40$ A^3 with 0.375 spacing. The box was centered at 29.47, 47.99 and 8.86, which is around the binding site of crizotinb in ALK receptor. For docking genetic algorithm was used with default set of parameters and 50 docked conformations were generated for each ligand.

3. Results and Discussion

3.1. Structural Properties

DLS measurements were performed to estimate the hydrodynamic size (d(H)) of the colloids. The measured d(H) of both Co-BMZ and Cu-BMZ is shown in Fig. 1. It can be seen that the Cu-BMZ particles distributed within the range of 150 nm whereas in the case of Co-BMZ samples, d(H) values are distributed between 100 and 700 nm, as identified from the double peak formation in the region. The double peaks may arise due to either the formation of intermediate products or due to the agglomeration of the particles [27]. In the present case, there is no possibility for the formation of intermediate products, due to the evaporation of alcohols at high temperature and the very less interaction between benzimidazole based metal complexes and water. On the other hand, if there is agglomeration of particles in the solution, with increasing time the dominant peak should move towards the higher particles size area. But, almost same d(H) values were obtained from the repeated DLS measurements over different time periods. So, presence of different size nanoparticles in the case of Co-BMZ may due to the different nucleation process during the spray of precursor solution. An in-depth analysis is required to identify such a process. In order to analyse the stability of prepared samples the zeta potential curves were recorded and are shown in Fig. 2. If zeta potential values are greater than 30 mV or lesser than −30 mV, the samples can be considered as stable [28]. In the present study, the obtained zeta potential value of 45 mV for Co-BMZ and 47.7 mV for Cu-BMZ ensures the stability of the prepared nanoparticles in the water medium.

The size and topology of the samples were studied using TEM and the obtained images are shown in Fig. 3. It is observed that the particle size of Co-BMZ is in the range between 100 and 400 nm, and for Cu-BMZ is in the range of 100 nm. The Cu-BMZ sample seems to be agglomerated and some patches are also visible (Fig. 3 (b)). The Co-BMZ nanoparticles are in cubic shape whereas most of the Cu-BMZ particles are in spheroid shape. If we ignore the hydration shell effect, the obtained particle sizes from the TEM images agree well with the DLS measurements.

3.2. Optical Properties

The recorded absorption spectra of the samples are shown in Fig. 4. Both the samples show good absorption in the region of 650 nm, which

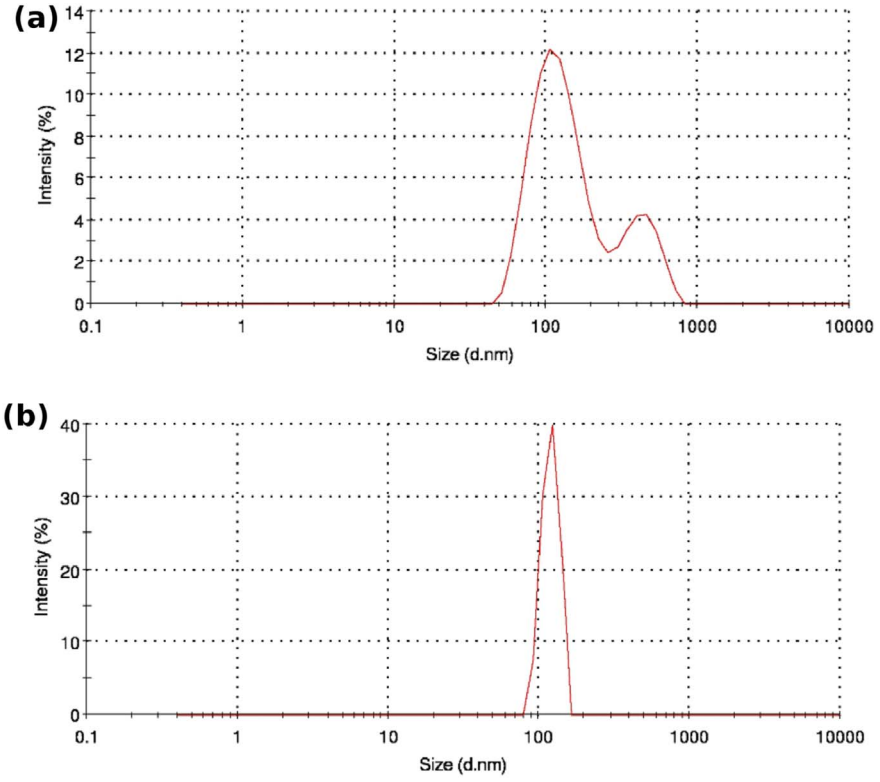

Fig. 1. Recorded hydrodynamic size of (a) Co-BMZ and (b) Cu-BMZ nanoparticles.

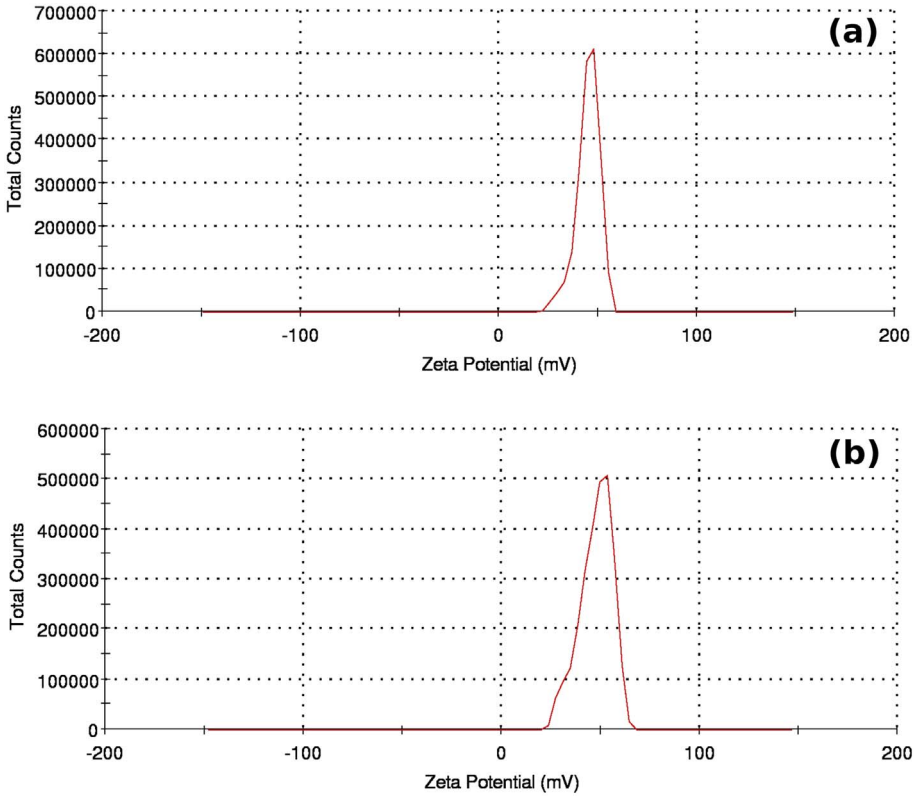

Fig. 2. The recorded zeta potential of (a) Co-BMZ and (b) Cu-BMZ nanoparticles.

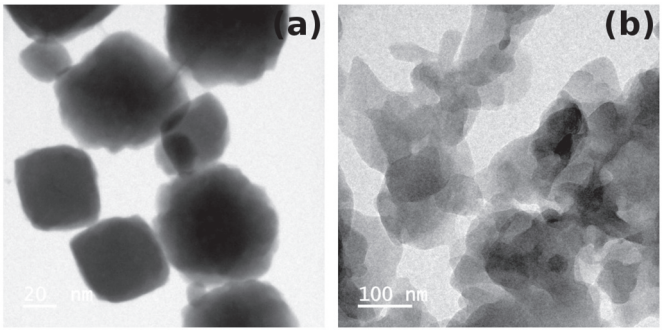

Fig. 3. TEM images of (a) Co-BMZ and (b) Cu-BMZ nanoparticles.

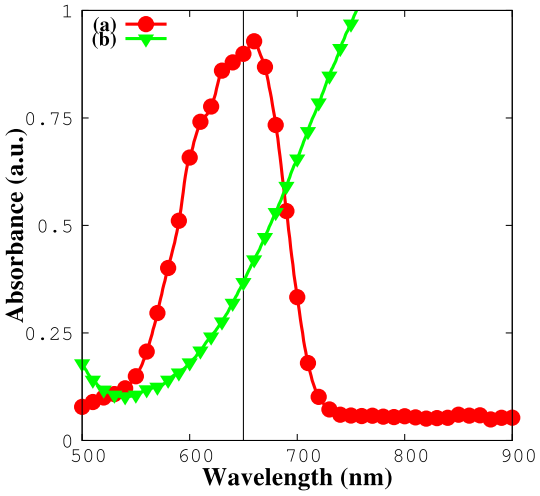

Fig. 4. Absorption spectra of (a) Co-BMZ and (b) Cu-BMZ nanoparticles.

is advantageous for thermo-optical studies performed using a source of same wavelength.

Interaction of CW laser with matter often induces thermal effect, that can affect the optical property of the medium. Such a phenomenon is called thermo-optical nonlinearity. In the present case, optical nonlinearity was used as a parameter to estimate thermal effects in the medium. i.e., higher the thermo-optical effect, higher would be the photothermal effect [29,30]. So, laser induced thermo-optical behavior of the samples were studied using Z-scan method [17]. The obtained OA and CA curves of both samples are shown in Fig. 5. In OA scans, the transmittance falls to minimum at focal point (Z = 0) indicates the presence of reverse saturable absorption (RSA) in the samples. The third order nonlinear optical property of metal organic samples studied using CW laser can be interpreted in terms of a five level electronic transition model. In which, upon laser irradiation the electrons in ground state (S_0) are excited to first electronic excited state (S_1) due to linear absorption. From which it can be excited to second electronic excited state (S_2) or may be relaxed to the ground state. But the presence metal ions degenerate the electronic levels, so most often in the case of metal complexes the electrons in (S_1) are further transferred to first triplet state (T_1). Now, further irradiation would make a transition from (T_1) to second triplet state (T_2). In such a scenario, depending upon the absorption cross sections of ground state and excited states, either a saturable absorption (SA) or reverse saturable absorption (RSA) will takes place in the sample. Depending upon the type of nonlinear absorption either a peak or valley corresponding to SA and RSA can be observed in OA Z-scan curves. Presence of RSA curves in both the cases, can be taken as the evidence that the samples possess higher excited state absorption cross section than the ground state absorption cross section. It is advantageous in the sense that unlike SA (in which material absorption tends to bleach at higher intensities), absorption in RSA materials increases with increase in laser intensity and induces a higher thermo-optical nonlinearity [31]. In CA scans, the Co-BMZ samples exhibit self-defocusing whereas the Cu-BMZ samples exhibits

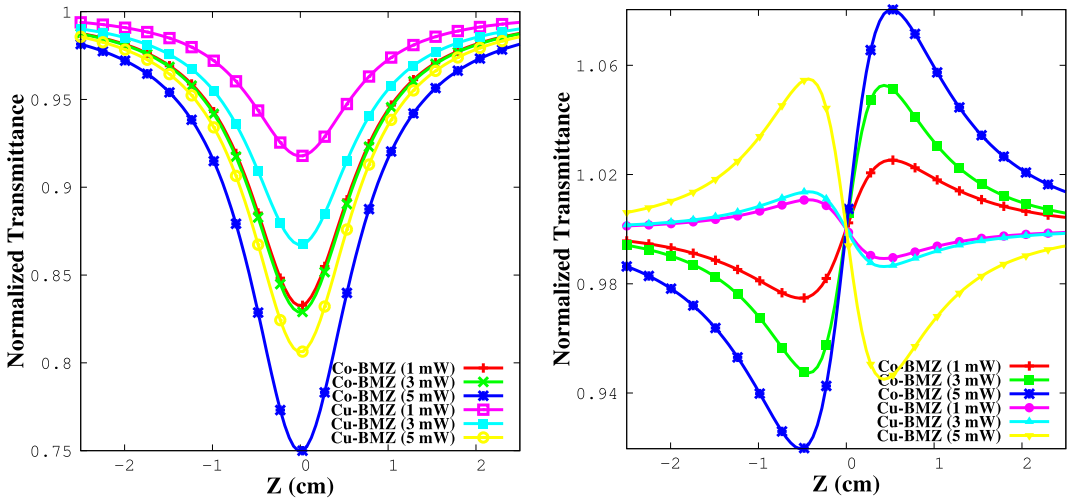

Fig. 5. Open (left) and closed (right) aperture Z-scan curves of the Co-BMZ and Cu-BMZ nanoparticles.

Table 1
Nonlinear optical parameters of Co-BMZ and Cu-BMZ nanoparticles.

Sample	β (m/W)	$n_2 \times 10^{-6}$ (m^2/W)	$\chi^{(3)} \times 10^{-6}$ (esu)
Co-BMZ (1 mW)	1.00	2.74	7.61
Co-BMZ (3 mW)	1.03	5.71	1.00
Co-BMZ (5 mW)	1.50	8.72	1.51
Cu-BMZ (1 mW)	0.49	−1.16	3.63
Cu-BMZ (3 mW)	0.79	−1.48	5.67
Cu-BMZ (5 mW)	1.16	−5.96	1.09

self-focusing phenomena. In CW regime thermal effects dominate over other mechanisms and the observed curves can be attributed to thermo-optical nonlinearity. In the present case, locally induced thermal gradient alters the refractive index of the Cu-BMZ samples, but the reversal of CA curves is observed in Co-BMZ samples, due to the high excited state population. The nonlinear absorptive and refractive coefficients extracted by fitting the experimental data were used to calculate the third order nonlinear susceptibility of the samples and is given in Table 1. It can be seen that the calculated susceptibility value increases with increase in input intensity, indicates that the thermo-optical behavior increases with increase in input intensity. Also, the higher values of nonlinear absorption coefficients reveal that the major nonlinear optical phenomena occur due to nonlinear absorption rather than nonlinear refraction.

3.3. Cytotoxicity Analysis

The effect of laser power on the cancerous (A549) and normal (NIH-3T3) cells was studied by irradiation of different laser powers, from 1 to 5 mW, for 4 min and the corresponding cell death was analysed using MTT assay. NIH-3T3 cells show minimal effect for all the three laser powers (1, 3, 5 mW), on the other hand A549 percentage of cell death increases with increase in input laser power and is shown in Fig. 6. It is a well known fact that the physical stability of the cancerous cells are much lower than the normal cells. On the other hand, a 5 mW CW laser profile contains lower energy which often create lower destruction to the normal cells [32]. So, the destruction of cancer cells alone by laser irradiation is advantageous for targeted therapy.

In order to study the cytotoxic effect of nanoparticles against the cancerous and non-cancerous cells, both the cell lines were treated with nanoparticles. Further, the cell lines were exposed to laser of power 5 mW for about 4 min to evaluate the effect of laser treatment. From which the IC_{50} values are extracted and given in Tables 2 and 3. Also, in vitro cytotoxic assays of the cell lines A549 and NIH-3T3 are shown in

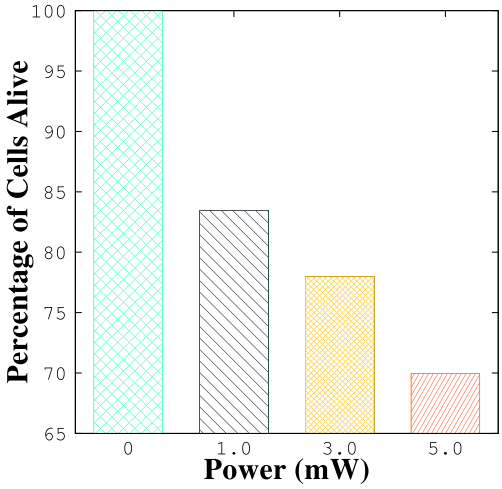

Fig. 6. Laser power vs the percentage of cells (A549) alive after irradiation.

Table 2
In vitro cytotoxicity assays for the complexes against human lung cancer cell line (A549).

Compound	IC_{50} values (μg/ml)
Co-BMZ	109 ± 0.05
Co-BMZ (laser treated)	86 ± 0.05
Cu-BMZ	95 ± 0.05
Cu-BMZ (laser treated)	60 ± 0.05

Table 3
In vitro cytotoxicity assays for the complexes against mouse embryonic fibroblast cell line (NIH/3T3).

Compound	IC_{50} values (μg/ml)
Co-BMZ	147 ± 0.05
Co-BMZ (laser treated)	132 ± 0.05
Cu-BMZ	178 ± 0.05
Cu-BMZ (laser treated)	165 ± 0.05

Figs. 7–10 and they clearly depict that the cells irradiated with laser light exhibit higher toxicity than the non-irradiated cells. The IC_{50} values revealed that the cancerous cells were destructed much than the normal cells in the same treatment conditions. Further, the obtained IC_{50} values of A549 cell lines indicates that Cu-BMZ nanoparticles show

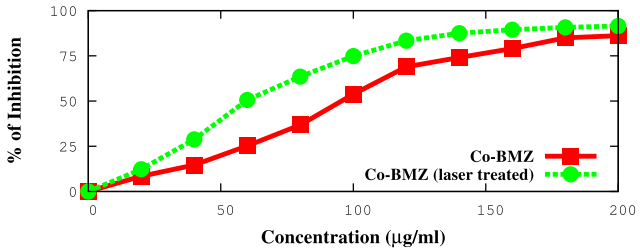

Fig. 7. In vitro cytotoxicity assays for Co-BMZ complex against human lung cancer cell line A549.

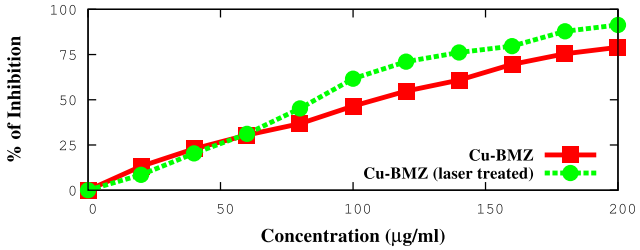

Fig. 8. In vitro cytotoxicity assays for Cu-BMZ complex against human lung cancer cell line A549.

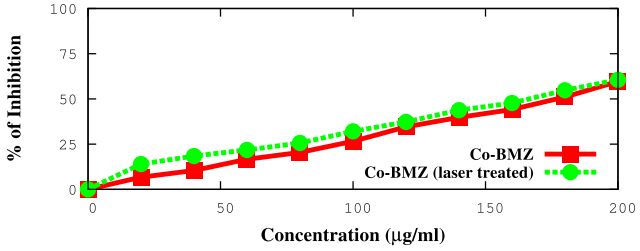

Fig. 9. In vitro cytotoxicity assays for Co-BMZ complex against mouse embryonic fibroblast cell lines NIH-3T3.

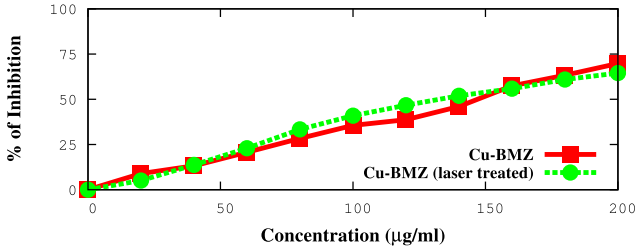

Fig. 10. In vitro cytotoxicity assays for Cu-BMZ complex against mouse embryonic fibroblast cell lines NIH-3T3.

better anticancer/PTT activity than the Co-BMZ nanoparticles due to their smaller particles size.

3.4. Morphological Analysis

Fluorescent microscopic study (Fig. 11) of AO/EB double-stained A549 human lung cancer cell line treated with Co-BMZ and Cu-BMZ nanoparticles for 24 h shows that the laser treatment induces majority of cell death through apoptosis and very fewer by necrosis. In the case of apoptosis, the cells underwent both early as well as late apoptosis. The most important characteristic of apoptosis are the occurrence of morphological changes during the cell death. The viable cells exhibit green fluorescence with normal cell features like uniform chromatin with intact cell membrane, whereas, the early apoptotic cells exhibit bright green region with yellowish green nuclear fragmentation, membrane bubbling formation of apoptotic bodies outside and the late

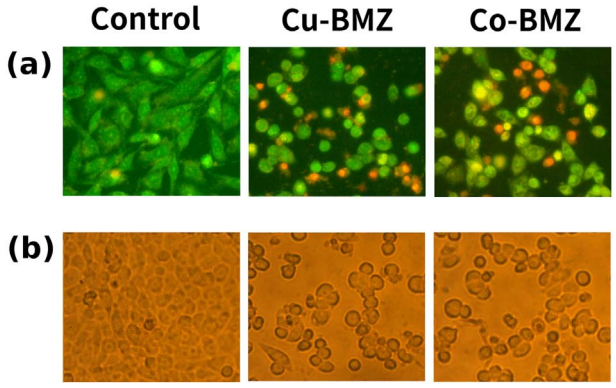

Fig. 11. (a) AO/EB: Control, Cu-BMZ and Co-BMZ treated A549 cells irradiated with laser. Green colour cells are live cells and red colour cells showing apoptotic morphology. (b) Light microscopic observation of control, Cu-BMZ and Co-BMZ treated A549 cells irradiated with laser. (For interpretation of the references to colour in this figure legend, the reader is referred to the web version of this article.)

apoptosis cells exhibited orange-yellow or red nuclei with condensed or fragmented chromatin. The cell destruction can be attributed to the reactive oxygen species (ROS) as well as to the laser-induced ROS [33]. Often the anticancer activity of the metal complexes arose due to ROS and it can be attributed to the redox potentials of the metal complexes [34]. The metal ions in the complexes tend to reduce the intercellular thiols like glutathione. Further reaction of reduced metal ions with molecular oxygen would generate the reactive superoxide radicals ($O_2^{\cdot-}$) which lead to the cell destruction [34,35]. So, in the present case, proton reduction of metal ions (Co and Cu) in the complexes induces ROS assisted destruction in the A549 cell lines. Further, smaller particle size favours more material to enter into the cell. Due to this, Cu-BMZ nanoparticles (with much smaller size) induced more destruction in the cell line. But during the laser irradiation, chances are high for microbubble formation, due to the heat stress generated by local thermal effects, than the laser-induced ROS [36]. So, in the present case, increment in cell destruction upon laser radiation can be attributed to the local thermal effects which was further contributed by the thermo-optical behavior of metal complexes in the operating wavelength.

3.5. Docking Analysis

In order to evaluate the binding mode of the synthesized ligands, docking analysis were performed using Autodock 4.2 [37]. Anaplastic Lymphoma Kinase (ALK) protein is chosen as the receptor for docking studies due to its potential anomaly in signaling cancer [38]. The simulations are validated by means of one-ligand run calculation using the original bound ligand 'crizotinib', which was extracted from the receptor. Since, the calculated root mean square deviation (RMSD) of scoring conformation falls under 1.6 , the method could be considered for the analysis of other compounds too. So, Co-BMZ and Cu-BMZ molecules are docked with ALK receptor using the same protocol used in the validation study. Docking studies for each molecule was performed for 2.5×10^6 energy evaluations and the docked conformations are analysed by means of bonding, energy and interaction between the ligand and ALK receptor. The poses are visualized by using PyMol and Chimera programs and the final coordinates of the ligand and receptor was saved in PDB format (Fig. 12). The docking scores are used to calculate the free binding energy and are given in Table 4. The docking results can be correlated with the anticancer analysis. Cu-BMZ complex shows better binding energy with ALK receptor, than Co-BMZ complex. The results are in agreement with the observed experimental results and indicate that the Cu-BMZ molecule fit well with the binding site of ALK receptor. The Cu-BMZ interacts with amino acids of ALK receptor, namely: GLY1269, ASP1270, LEU1256, LEU1198, LEU1122, LEU1196, GLU1197, ALA1148, LYS1150, MET1199, ARG1253 and ASN1254.

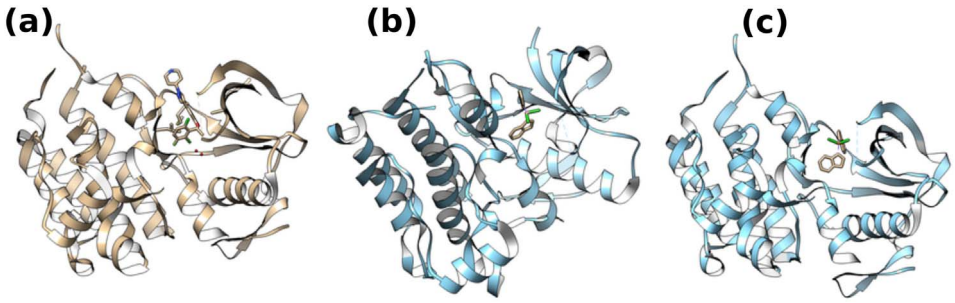

Fig. 12. Docking positions of (a) crizotinib, (b) Co-BMZ and (c) Cu-BMZ molecules with ALK receptor.

Table 4
Docking scores and IC_{50} values of Co-BMZ and Cu-BMZ complexes.

	Co-BMZ	Cu-BMZ
Dock score	−6.80	−7.24
IC_{50} value	95	109

Whereas, the Co-BMZ complex interacts with amino acids of LEU1122, EU1196, ALA1148, LEU1196, MET1199, LEU1256, ARG1253, ASP1270 and ASN1254.

4. Conclusion

Benzimidazole based metal organic nanoparticles were synthesized by simple reprecipitation method and subjected to DLS, zeta potential and TEM analyses. Results showed that the synthesized particle size is in the range between 100 and 400 nm in the case of Co-BMZ and 100 nm in the case of Cu-BMZ. Both the particles are found to be stable from the zeta potential analysis. The linear and nonlinear absorptive studies indicate that the metal complexes have good absorption in the 650 nm region and shows reverse saturable absorption. The nonlinear optical parameters increase with increase in laser power corresponds to higher thermal effects. PTT and docking studies reveal that the Cu-BMZ samples possess better anti-cancer activity than the Co-BMZ particles. The size and interaction energy of the Cu-BMZ particles can be accounted for their potential activity. Further, the irradiated cells exhibit higher toxicity than the treated cells, corresponding to the thermal effects due to the laser irradiation.

Acknowledgments

The authors acknowledge the financial assistance from the School of Physics, provided by DST-FIST (Order No.: SR/FIST/PSI-204/2015 (c)) for the establishment of research facilities. Further, one of the authors P.A. Praveen thank the UGC-BSR Govt. of India for financial assistance in the form of 'Research Fellowship in Science for Meritorious Students' (F.4-1/2006/7-197/2007(BSR)).

References

[1] Cancer Statistics from National Cancer Institute, https://www.cancer.gov/about_cancer/understanding/statistics, accessed: 2017-03-07.
[2] C. Jungk, D. Chatziaslanidou, R. Ahmadi, D. Capper, J.L. Bermejo, J. Exner, A. von Deimling, C. Herold-Mende, A. Unterberg, BMC Cancer 16 (1) (2016) 81.
[3] K. Hauner, P. Maisch, M. Retz, Der Urologe. Ausg. A 56 (4) (2017) 472.
[4] D. De Miguel, J. Lemke, A. Anel, H. Walczak, L. Martinez-Lostao, Cell Death Differ. 23 (5) (2016) 733.
[5] A. Espinosa, A.K. Silva, A. Sánchez-Iglesias, M. Grzelczak, C. Péchoux, K. Desboeufs, L.M. Liz-Marzán, C. Wilhelm, Adv. Healthc. Mater. 5 (9) (2016) 1112.
[6] Y. Chen, K. Ai, J. Liu, X. Ren, C. Jiang, L. Lu, Biomaterials 77 (2016) 198.
[7] X. Yao, X. Niu, K. Ma, P. Huang, J. Grothe, S. Kaskel, Y. Zhu, Small 13 (2) (2017) 1602225.
[8] Z. Li, H. Huang, S. Tang, Y. Li, X.-F. Yu, H. Wang, P. Li, Sun, Biomaterials 74 (2016) 144.
[9] X. Zhu, W. Feng, J. Chang, Y.-W. Tan, J. Li, M. Chen, Y. Sun, F. Li, Nat. Commun. 7 (2016) 10437.
[10] Y.-W. Chen, Y.-L. Su, S.-H. Hu, S.-Y. Chen, Adv. Drug Deliv. Rev. 105 (2016) 190–204.
[11] D. Wang, C. Hou, L. Meng, J. Long, J. Jing, D. Dang, Z. Fei, P.J. Dyson, J. Mater. Chem. B 5 (7) (2017) 1380.
[12] S. Zhang, C. Sun, J. Zeng, Q. Sun, G. Wang, Y. Wang, Y. Wu, S. Dou, M. Gao, Z. Li, Adv. Mater. 28 (40) (2016) 8788.
[13] U. Freudenberg, Y. Liang, K.L. Kiick, C. Werner, Adv. Mater. 28 (40) (2016) 9013.
[14] J. Kim, J. Kim, C. Jeong, W.J. Kim, Adv. Drug Deliv. Rev. 98 (2016) 99.
[15] B. Zhou, Y. Li, G. Niu, M. Lan, Q. Jia, Q. Liang, ACS Appl. Mater. Interfaces 8 (44) (2016) 29899.
[16] B. Zhang, Y. Shan, K. Chen, Mater. Chem. Phys. 193 (2017) 82.
[17] P.A. Praveen, R. Ramesh Babu, K. Jothivenkatachalam, K. Ramamurthi, Spectrochim. Acta A Mol. Biomol. Spectrosc. 150 (2015) 280.
[18] P.A. Praveen, R. Ramesh Babu, K. Ramamurthi, Spectrochim. Acta A Mol. Biomol. Spectrosc. 173 (2017) 800.
[19] W. Wang, L. Wang, Y. Li, S. Liu, Z. Xie, X. Jing, Adv. Mater. 28 (42) (2016) 9320.
[20] Y. Yang, J. Liu, C. Liang, L. Feng, T. Fu, Z. Dong, Chao, ACS nano 10 (2) (2016) 2774.
[21] A.H. El-Masry, H. Fahmy, S. Ali Abdelwahed, Molecules 5 (12) (2000) 1429.
[22] T.D. Penning, G.-D. Zhu, V.B. Gandhi, J. Gong, X. Liu, Shi, J. Med. Chem. 52 (2) (2008) 514.
[23] I.H. El-Sayed, X. Huang, M.A. El-Sayed, Cancer Lett. 239 (1) (2006) 129.
[24] A.K. Gupta, M. Gupta, Biomaterials 26 (18) (2005) 3995.
[25] T. Mosmann, J. Immunol. Methods 65 (1) (1983) 55.
[26] D. Spector, R. Goldman, L. Leinwand, Culture and biochemical analysis of cells. Vol. 1: A Laboratory Manual, Cold Spring Harbor Laboratory Press, Cold Spring Harbor, NY, 1998.
[27] J. Lim, S.P. Yeap, H.X. Che, S.C. Low, Nanoscale Res. Lett. 8 (2013) 381.
[28] D. Li, M.B. Müller, S. Gilje, R.B. Kaner, G.G. Wallace, Nat. Nanotechnol. 3 (2) (2008) 101.
[29] T.H. Jamieson, Opt. Eng. 20 (2) (1981) 156.
[30] C. Schmidt, A. Chipouline, T. Pertsch, A. Tnnermann, O. Egorov, F. Lederer, L. Deych, Opt. Express 16 (9) (2008) 6285.
[31] S. Hirata, K. Totani, T. Yamashita, C. Adachi, M. Vacha, Nat. Mater. 13 (10) (2014) 938.
[32] D. Wirtz, K. Konstantopoulos, P.C. Searson, Nat. Rev. Cancer 11 (7) (2011) 512.
[33] J. Yoon, S.-w. Ryu, S. Lee, C. Choi, Sci. Rep. 5 (2015) 8231.
[34] A. Sirbu, O. Palamarciuc, M.V. Babak, J.M. Lim, Dalton Trans. 46 (12) (2017) 3833.
[35] J. Wang, C. Li, Q. Zhou, W. Wang, Y. Hou, B. Zhang, X. Wang, Catal. Sci. Technol. 6 (24) (2016) 8482.
[36] V.P. Pattani, J. Shah, A. Atalis, A. Sharma, J.W. Tunnell, J. Nanopart. Res. 17 (1) (2015) 20.
[37] AutoDock 4.2 - Docking Software, http://autodock.scripps.edu/resources/references, accessed: 2017-03-07.
[38] T.H. Marsilje, W. Pei, B. Chen, W. Lu, Uno, J. Med. Chem. 56 (14) (2013) 5675.